Finite Element Model of Pulsed Laser Welding

A newly developed model correlated with an experiment has shown laser beam energy distribution and absorptivity greatly affects laser weld dimensions

BY M. R. FREWIN AND D. A. SCOTT

ABSTRACT. A three-dimensional finite element model of the heat flow during pulsed laser beam welding is presented. The heat transfer and parametric design capabilities of the finite element code ANSYS were employed for this purpose. The model calculates transient temperature profiles and the dimensions of fusion and heat-affected zones (HAZ). Temperature-dependent thermophysical properties and experimentally measured beam profiles are incorporated. Model calculations are compared and then calibrated with experimental results of pulsed laser welds. The results suggest that temperature profiles and weld dimensions are strong functions of the absorptivity and energy distribution of the laser beam. For this reason, it is essential to incorporate an accurate description of the heat source.

Introduction

Laser beam welding is a field of growing importance in industry. Pulsed laser welding offers the advantage of very low heat input to the weld, resulting in low distortion and the ability to weld heat-sensitive components. While there have been several numerical and analytical models that have sought to elucidate the physical mechanisms involved in the continuous-wave laser welding process, there exist few models of pulsed laser welding. These are reviewed below. The main reason for this apparent scarcity lies in the complexity of the laser-material interaction process. Pulsed laser welding in this article refers to the low repetition rate regime in which significant resolidification of the workpiece occurs between laser pulses. As the laser beam intermittently interacts with the workpiece over very short time intervals, very rapid heating and cooling cycles result. The weld bead is the product of a number of overlapping spot welds, and every point in the weld area experiences a complex series of thermal cycles during the passage of the laser beam. This complexity implies that analytical modeling techniques are almost impossible. The numerical model, therefore, is the preferred option, although the analysis requires a very large number of small time steps — much smaller than those needed for the continuous analysis.

M. R. FREWIN is with the Department of Materials Engineering, University of Wollongong, Wollongong, NSW, Australia, and D. A. SCOTT is with the Commonwealth Scientific and Industrial Research Organisation, Industrial Laser Centre, Division of Manufacturing Technology, Lindfield, NSW, Australia.

Previous Models of Laser Welding

Rosenthal's solutions (Ref. 1) represent the starting point of analytical solutions applied to welding techniques in general. It was not until 1973 that Swift-Hook and Gick (Ref. 2) developed the first heat transfer model for continuous laser welding. In a similar manner to Rosenthal, the laser beam was modeled as a moving line source. It was assumed that the melting temperature isotherm determined the location and shape of the fusion zone. The width and depth of the fusion zone were then related to the laser power and velocity of the workpiece. Since the formation of a keyhole was neglected, their model produces only partial agreement with experimental results and applies mainly to conduction laser welding. Convective flow in the weld pool was not considered.

In 1976, Klemens (Ref. 3) produced a more sophisticated model of the continuous laser welding process. The model assumes a plasma-filled keyhole, which is held open by a balance between vapor pressure within the keyhole, surface tension and hydrodynamic pressure in the molten region surrounding the keyhole.

Three-dimensional convective flow in the weld pool was extensively investigated in 1976 by Andrews and Atthey (Ref. 4). Although four distinct driving forces for weld pool convection exist — buoyancy, gravity, surface tension and plasma forces — this model incorporates only the effects of gravity and surface tension. The underlying assumptions are that the vapor pressure inside the keyhole is taken to be equal to the atmospheric pressure and 100% of the incident power is absorbed at the surface of the workpiece. In practice, the former assumption is valid only for shallow keyholes, whereas the latter simplification is unjustified. Absorptivity is a function of a number of variables, such as the nature of the surface, the level of oxidation, surface temperature, power density of the beam and amount of plasma present. The assumption of a constant absorptivity is unlikely to be realistic.

In 1977, Cline and Anthony (Ref. 5) integrated the point source over the workpiece surface to yield a Gaussian power distribution, eliminating singularities in the temperature calculations and showing that spot size has a strong influ-

KEY WORDS

Nd:YAG Laser
Pulsed Laser
Laser Welding
Numerical Modeling
Steel
Absorptivity
Energy Distribution
Optical Fiber

ence on the maximum temperature attained by the workpiece. The model assumes 100% absorption and calculates an exponential decrease of the temperature in the vertical direction. Conduction and keyhole welding conditions were both considered, whereas weld pool convection was not included in the model.

In 1986, convective flow was examined by Davis, *et al*. (Ref. 6). Their model starts with the basic assumption that the Peclet number, which is the ratio of convected to conducted heat, is small. It also assumes two-dimensional convective flow, independent of keyhole depth, modeled by solving the Navier-Stokes equations of motion. A simpler approach is to compensate for the weld pool convective heat transfer with an artificially high thermal conductivity for the material in the weld pool. Typically, a thermal conductivity of as much as ten times its actual value at the solidus temperature has been used in conventional welding models (Ref. 7). Unfortunately, this means that various values of conductivity for the molten material must be trialed until a reasonable weld pool shape is obtained. Anisotropic conductivities can also be used for this purpose but have not been applied to laser welding models. Other significant modeling efforts are also presented (Refs. 8–13).

The difficulties associated with analytical models of the laser welding process may be partially overcome by employing numerical rather than purely analytical techniques. Detailed information on temperature-dependent thermophysical properties is difficult to obtain, however, so most numerical modeling efforts have used constant or assumed values for selected thermophysical properties.

Mazumder and Steen (Ref. 14) developed the first numerical model of the continuous laser welding process. This model implements the finite difference technique for a Gaussian beam intensity distribution and starts with the assumption that the absorptivity of the incident radiation below the boiling point is 20%. While convective flow in the weld pool and the temperature dependence of the thermophysical properties are not considered, the nonlinearities of convection and radiation to surroundings are included in the model. The absorptivity of the laser radiation is considered to be 100% when the temperature exceeds the boiling point. As a result, matrix points remain in the conducting network at fictitiously high temperatures to simulate the convection and radiation heat transfer mechanisms within the plasma. Beer-Lambert's Law describes attenuation of the laser radiation within the keyhole. The model can be used to predict temperature distributions, the size and shape of fusion and heat-affected zones, maximum welding speeds and the effect of workpiece thickness. Other published numerical/analytical models are also listed (Refs. 15–19).

During pulsed laser welding, the material is heated intermittently with a succession of short-duration pulses to produce a series of overlapping spot welds. Consequently, the material is subjected to a large number of thermal cycles. Predictions of accurate heating and cooling rates using analytical methods are very difficult to obtain. Therefore, a two-dimensional numerical model employing the finite difference technique was developed by Zacharia, *et al*. (Ref. 20). This model describes two-dimensional convective flow and heat transfer in the fusion zone for a Gaussian heat source, assuming that the flow is primarily driven by the gradient of the surface tension and that vaporization effects are negligible. This numerical model correlates calculated thermal cycles and cooling rates with features of the solidification structure. Temperature-dependent thermophysical properties are not included in this model. This added complexity was only partially considered by Russo, *et al*. (Ref. 21). Their two-dimensional numerical analysis of the pulsed laser welding process assumes surface tension to vary linearly with temperature, while kinematic viscosity is assumed to vary exponentially with temperature.

Further published research on modeling pulsed laser welding is limited. Vishnu, *et al*. (Ref. 22), developed a three-dimensional solution for the temperature distribution due to an instantaneous, stationary Gaussian heat source. This solution was then extended to consider a single, moving heat source and, finally, a series of heat pulses. These theoretical calculations were compared with empirical results for gas tungsten arc (GTA) welds, but may be used to describe pulsed laser welding. Gellert and Egli (Ref. 23) developed a basic one-dimensional model that describes the melting of copper by a pulsed heat source. Jette and Benson (Ref. 24) constructed a one-dimensional model of pulsed laser heating of optical surfaces, while Arutyunyan, *et al*. (Ref. 25), developed a general hydrodynamic model of the interaction of pulsed radiation with matter.

Previously published work indicates several improvements that may be made to these models:

1) Experimental determination of the intensity profile of the laser beam, which is then incorporated into the model.

2) Minimization of the mesh size near the heat source.

3) Implementation of finite element codes such as ANSYS, ABAQUS or NASTRAN to develop adaptive meshing and remeshing schemes.

4) The development of more hybrid analytical/numerical models.

The Present Model

The approach here has been to solve just the energy balance equation with appropriate initial and boundary conditions. The method employed uses realistic temperature-dependent variables, experimentally measured laser beam intensity distributions, and requires only one "calibration" factor to match model predictions with experiment for a wide range of conditions. Because pulsed laser welding involves very rapid melting and resolidification (rather than a permanent liquid pool), convective redistribution of heat in the weld pool is minimal and may be neglected.

This paper presents a new three-dimensional model of the laser welding process utilizing the efficient solution procedures of the finite element code ANSYS on an SGI Challenge L series workstation. The results of this model are compared with experimental results. A pulsed Nd:YAG laser of wavelength 1.06 μm was used to generate single spot welds on AISI 1006 steel plates. The physical dimensions of the fusion zone (FZ) and weld zone (WZ = FZ + HAZ) were measured and compared with the predictions of the model.

Physical Description of the Model

A moving, pulsed laser beam with an experimentally determined energy distribution strikes the surface of a finite three-dimensional AISI 1006 steel plate. The power density is sufficient to form a bead-on-plate laser weld. The dimensions of the plate and heat source are shown in Fig. 1.

The following assumptions were made in the formulation of the finite element model:

1) The laser beam is incident at an angle θ to the surface of the workpiece. Laser welding with fiber optics is often performed at an angle θ to prevent back-reflections from the workpiece damaging the delivery optics. This is particularly so when welding highly reflective materials such as aluminum and copper.

2) The workpiece is initially at 20°C (68°F). Both the laser beam and the coordinate mesh are fixed and the work-

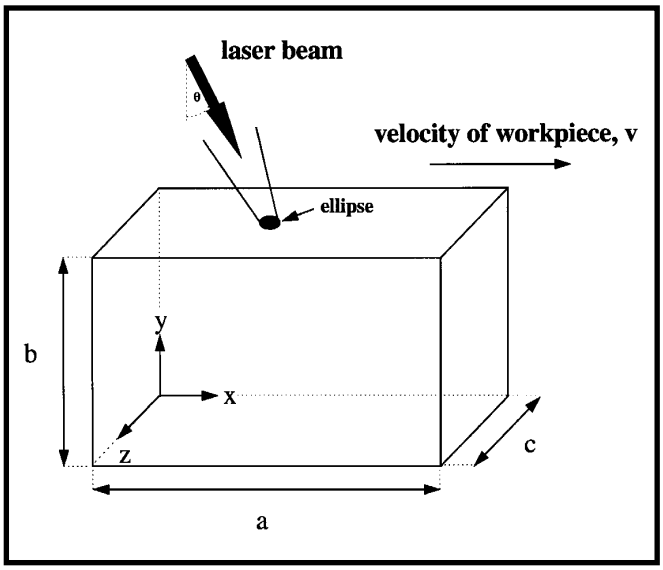

Fig. 1 — Finite plate heated over an elliptical region by a laser beam. The laser beam and the coordinate system are fixed and the workpiece moves at velocity v.

piece moves in the positive x-direction with a constant velocity, v.

3) For temperatures below the boiling point of the material (*i.e.*, 2860°C [5180°F] for steel), a proportion of the incident radiation is absorbed, determined by the "effective absorptivity" described below, and the rest is reflected. Above the boiling point, 70% of this absorbed radiation is assumed to be further absorbed by the vapor/plasma, and the remaining 30% is transmitted through the vapor according to Beer-Lambert's Law. The final proportion remaining at the walls of the keyhole is fully absorbed by the material through a Fresnel interaction. The vapor/plasma absorptivity was determined by comparing experiment with theory, since below 70% vaporization was not maintained in the model, above 70% boiling was too rapid and the resulting melt pool was too deep and too wide. Attenuation according to Beer-Lambert's Law is described by

$$P = P' \exp(-\alpha L) \quad (1)$$

where α is the absorption coefficient (m^{-1}), which was considered to be independent of position within the keyhole. For low-carbon steel, Mazumder and Steen (Ref. 14) suggest a value of 800 m^{-1}. P is the beam power reaching a depth L, and P' is the incident power.

4) When the temperature of a node exceeds the boiling point of the steel, it remains in the mesh at the vaporization temperature to simulate the presence of a plasma-filled keyhole, and the thermophysical properties used are those for iron vapor at 2860°C (Table 1). This approach is similar to the one adopted by Mazumder and Steen (Ref. 14).

5) All thermophysical properties are considered to be temperature dependent. These properties are shown in Table 1: thermal conductivity, specific heat and emissivity according to Brown and Song (Ref. 26) and density according to Kim (Ref. 27).

6) The latent heat of fusion is simulated by an artificial increase in the liquid-specific heat according to Brown and Song (Ref. 26).

7) As pulsed laser welding involves very rapid melting and solidification, convective redistribution of heat within the weld pool is not as significant as it is in other processes where a liquid pool is permanent. Convective flow of heat, therefore, is neglected.

Table 1 — Thermophysical Properties Used in the Finite Element Model

Temperature °C	Temperature (°F)	Thermal Conductivity (W m^{-1} K^{-1})	Specific Heat (J kg^{-1} m^{-3})	Emissivity	Density (kg m^{-3})
0	(32)	51.9	450	0.2	7872
75	(167)	51.3	486	0.35	7852
100	(212)	51.1	494	0.4	7845
175	(347)	49.5	519	0.44	7824
200	(392)	49	526	0.45	7816
225	(437)	48.3	532	0.46	7809
275	(527)	46.8	557	0.47	7763
300	(572)	46.1	566	0.48	7740
325	(617)	45.3	574	0.48	7717
375	(707)	43.6	599	0.5	7727
400	(752)	42.7	615	0.51	7733
475	(887)	40.2	662	0.53	7720
500	(932)	39.4	684	0.54	7711
575	(1067)	36.6	749	0.55	7680
600	(1112)	35.6	773	0.56	7669
675	(1247)	32.8	846	0.57	7636
700	(1292)	31.8	1139	0.57	7625
730	(1346)	30.1	1384	0.58	7612
750	(1382)	28.9	1191	0.58	7602
775	(1395)	27.5	950	0.58	7590
800	(1472)	26	931	0.58	7578
1000	(1832)	27.2	779	0.59	7552
1500	(2732)	29.7	400	0.6	7268
1540	(2804)	29.7	400	0.6	7218
1590	(2894)	29.7	847	0.6	7055
1840	(3344)	29.7	847	0.6	6757
1890	(3434)	29.7	400	0.6	6715
2860	(5180)	29.7	400	0.62	5902

These properties are linearly interpolated for the intermediate temperatures.

Mathematical Description of the Model

The spatial and temporal temperature distribution T(x,y,z,t) satisfies the following differential equation for three-dimensional heat conduction in a domain D:

$$\frac{\partial}{\partial x}\left(k_x \frac{\partial T}{\partial x}\right) + \frac{\partial}{\partial y}\left(k_y \frac{\partial T}{\partial y}\right) + \frac{\partial}{\partial z}\left(k_z \frac{\partial T}{\partial z}\right) + Q = \rho c\left(\frac{\partial T}{\partial t} - v\frac{\partial T}{\partial x}\right) \quad (2)$$

where

- (x,y,z) = coordinate system attached to the heat source
- Q = power generation per unit volume in the domain D (W m^{-3})
- k_x, k_y, k_z = thermal conductivity in the x, y and z directions (W m^{-1} K^{-1})
- c = specific heat capacity (J kg^{-1} K^{-1})
- ρ = density (kg m^{-3})
- t = time (s)
- v = velocity of workpiece (m s^{-1})

The initial condition is

$$T(x,y,z,0) = T_0 \quad \text{for } (x,y,z) \in D. \quad (3)$$

The essential boundary condition is

$$T(0,y,z,t) = T_0 \quad (4)$$

on the boundary S_1 for $(y,z) \in S_1$ and $t > 0$. This condition prescribes nodal temperatures at the flow inlet. S_1 represents the inlet surface. The natural boundary conditions can be defined by

$$k_n \frac{\partial T}{\partial n} - q + h(T - T_0) + \sigma\varepsilon(T^4 - T_0^4) = 0 \quad (5)$$

on the boundary S_2 for $(x,y,z) \in S_2$ and $t > 0$. S_2 represents those surfaces that are subject to radiation, convection and imposed heat fluxes. A special case of the imposed heat flux is the adiabatic condition, which represents insulated or symmetry surfaces. Other symbols are defined as

- k_n = thermal conductivity normal to S_2 (W m^{-1} K^{-1})
- h = heat transfer coefficient for convection (W m^{-2} K^{-1})
- σ = Stefan-Boltzmann constant for radiation (5.67×10^{-8} W m^{-2} K^{-4})
- ε = emissivity
- T_0 = ambient temperature (K)

$$q = \delta q_e \quad (6)$$

where

- q_e = $q_e(x,y,z)$ = experimentally determined heat flux normal to S_2 (W m^{-2})
- δ = Kronecker delta
  = 1 for pulse on
  = 0 for pulse off.

The inclusion of temperature-dependent thermophysical properties and a radiation term in the above boundary condition makes this type of analysis highly nonlinear. Since the incorporation of radiation effects was found to increase solution times by as much as three times, Vinokurov's (Ref. 28) empirical relationship for welding hot-rolled steel plates was used:

$$h = 2.4 \times 10^{-3} \varepsilon T^{1.61} \quad (7)$$

Equation 7 combines the effects of radiation and convection into a "lumped" heat transfer coefficient. The associated loss in accuracy using this relationship is estimated to be less than 5%.

Numerical Description of the Model

The finite element code ANSYS (Revision 5.2) provides a convenient means of numerically modeling pulsed laser welding. A system with an infinite number of unknowns (the response at every location in the system) can be transformed into one that has a finite number of unknowns related to each other by elements of finite size.

The solution technique is then chosen, depending on the type of problem. In the present case, the thermal history of a bead-on-plate weld is required, so a transient thermal analysis must be performed. This requires an integration of the heat conduction equation with respect to time. In the finite element formulation, this equation can be written for each element as

$$[C(T)]\{\dot{T}\} + [K(T)]\{T\} + \{V\} = \{Q(T)\} \quad (8)$$

where

- $[K]$ = conductivity matrix
- $[C]$ = specific heat (or capacitance) matrix
- $\{T\}$ = vector of nodal temperatures
- $\{\dot{T}\}$ = vector of time derivative of $\{T\}$
- $\{V\}$ = velocity vector for the moving workpiece
- $\{Q\}$ = nodal heat flow vector.

This equation is simply the vector and matrix equivalent of Equation 2 (Ref. 29). Standard variational techniques are then applied to solve these system equations. This is accomplished through the Crank-Nicholson/Euler theta integration method in which the equations are solved at discrete time points within the transient. The difference between any two time points is known as the integration time, which is specified by the user. If necessary, the time step can be varied during the transient. The program's automatic time-stepping feature can be employed to automatically increase or decrease the integration time step based upon response conditions (Ref. 29).

The first iteration in the solution procedure solves the system equations at an assumed starting temperature (which may be specified by the user), and subsequent iterations use temperatures from previous iterations to calculate the thermal conductivity and specific heat matrices. The iterative process continues until a converged solution is achieved, *i.e.*, when user-defined convergence criteria are met. Convergence checking can be based on the out-of-balance heat flow vector and/or the temperature increment from one iteration to the next. The number of iterations necessary for an accurate solution depends upon the nonlinearity of the problem. An analysis with temperature-dependent thermophysical properties normally requires two or three iterations to converge, while ten or more iterations may be necessary for analyses dominated by radiation heat transfer.

The solution data are in the form of nodal temperatures and heat flows. These data may be used in the postprocessing phase to produce displays of temperature contours (isotherms). Other postprocessing options may be used to extract more specific information, such as the thermal gradient and thermal flux at nodes and element centroids. This information can be displayed either graphically or in tabular form.

Modeling Results

The results of the ANSYS program can be displayed in many ways. Since the program is capable of calculating the temperature at any nodal point in the material as a function of time, different modes of presentation of the results need to be selected to assess the ability of the model to predict experimentally measurable quantities. This comparison of experiment with theory and the consequent modification of the various parameters that represent physical processes in the model may allow the estimation of the relative importance and role of the complex physical interactions that govern pulsed laser welding.

Initial comparisons of experiment and theory were done on single-pulse spot welds. The finite element mesh is shown in Fig. 2. As the heat source is symmetric about the x-y plane, only half the heat source is considered. The mesh is linearly graded from fine to coarse, according to the expected reduction in temperature gradient on moving away from the heat source. An error estimation technique based on the discontinuity of the heat flux between elements was employed to achieve a calculation accuracy of ±5%. As a result, this mesh provides an optimum balance between solution time and accuracy.

The model was run for both the duration of a single laser pulse and the subsequent cooling period. An innovative technique was implemented to transfer and store the large amount of data generated during the solution procedure. This data includes the depth of the 1540 and 730°C (2804 and 1346°F) isotherms that approximately represent the fusion zone (FZ) and weld zone (WZ) boundaries, respectively. Exposure of sheet steel to a single laser pulse formed a spot

weld, which was then sectioned and prepared so the FZ and WZ dimensions could be measured. These comparisons were conducted for a wide range of laser welding parameters and the results of selected experiments are given in the following section.

The laser system used to generate the experimental results in this paper was a LASAG KLS522 pulsed Nd:YAG laser equipped with a 10-m fiber-optic cable and a LL-BK1 processing head. This head incorporates standard two-element optics to refocus the beam emerging from the optical fiber. Small amounts of spherical aberration inherent in this design gave rise to different intensity distributions as a function of focal position.

It was found that two of the most sensitive inputs to the model were the shape of the intensity profile of the laser beam and the absorptivity of the beam at the surface of the workpiece. To ensure accurate intensity distributions, the cross-sectional intensity profiles of the pulsed Nd:YAG laser beam used in the experiments were measured over a wide range of laser parameters using a commercial Spiricon LBA-100 laser beam analyzer (Refs. 30, 31). The data as measured by this system were used to generate a matrix of power density values that were then used as input data for the model. An example of one of these measured profiles is shown in Fig. 3. Although this profile has an approximately conical shape, measured intensity profiles under other laser conditions (focal positions) were found to be approximately Gaussian, top-hat or even donut shaped.

To demonstrate the sensitivity of the model to intensity distribution, the model was run using the measured profile — Fig. 3. The model was then run using an artificially generated top-hat profile of the same full width at half maximum (FWHM) and the same total energy as the measured profile. A comparison of the predicted depths and diameters of the FZ and WZ is shown in Table 2. This clearly indicates that unless the correct intensity profile is used as input into the model, large discrepancies between model predictions and experimental results will occur. The results of numerical and analytical models of the laser welding process that assume line, Gaussian or top-hat profiles of intensity distribution must, therefore, be treated with caution. All these calculations have used experimentally measured energy distributions.

Comparison of Experiment and Theory

Using a single optical fiber (0.6-mm-diameter, step index) and a 100-mm focal length processing head (Lasag LL-BK1), single laser pulses were delivered onto 0.9-mm AISI 1006 steel. Laser pulses of duration 3 ms, energy 7 J and repetition rate 20 Hz were incident on the workpiece, moving fast enough to ensure no overlap of spot welds (3000 mm/min). Thus, the effect of a single laser spot could be examined. The beam was incident on the surface of the material at an angle of 10 deg and a focal scan was made from –5 mm (focal point beneath the surface) to 5 mm (above the surface) in increments of 1 mm. Figure 4 shows a micrograph of the cross section of one of the spot welds (focus 0 mm). From such a micrograph, the depth and diameter of the FZ and WZ may be measured. Just as this laser spot weld was physically sectioned, a section through the centerline of the model can be taken.

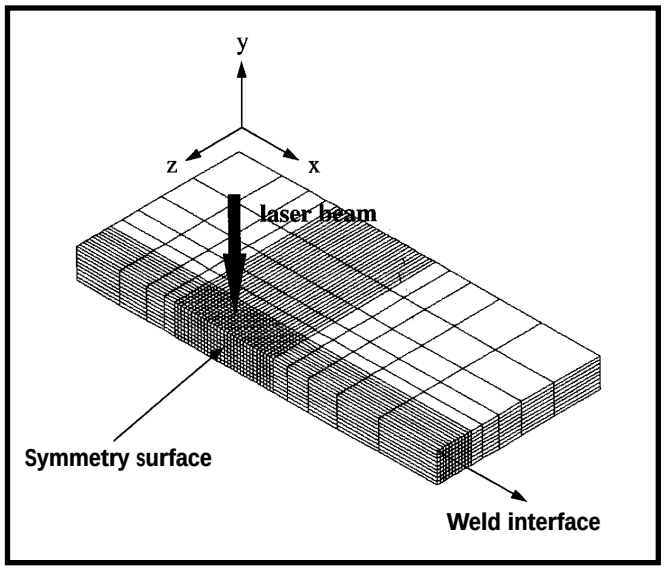

Fig. 2 — 11 x 0.9 x 5 mm finite element mesh consisting of five 616 eight-noded elements. Each element in the fine section of the mesh has a volume of 0.1 x 0.1 x 0.1 mm, and the mesh remains fixed with respect to the laser beam.

ANSYS model predictions of the FZ and WZ boundaries are superimposed on this micrograph. These isotherms represent the positions that have been heated up to maximum temperatures of 1540 and 730°C, respectively.

The model was also run for the other focal positions. The temperature of each nodal point within the solid was calculated as a function of time. For each

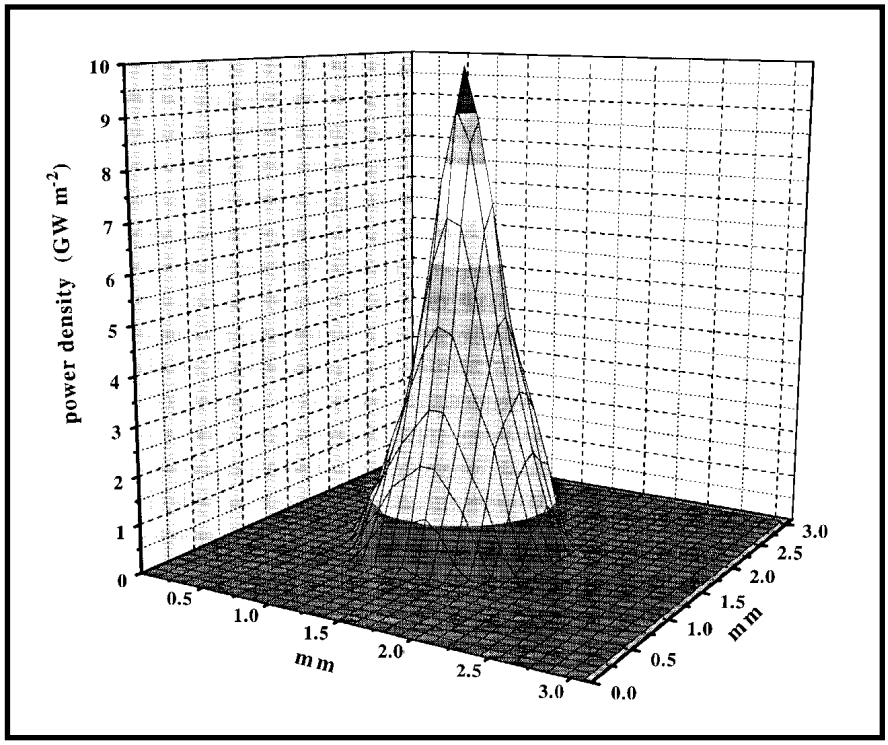

Fig. 3 — Intensity profile of Nd:YAG laser beam. Laser conditions: 7 J, 3 ms, focus 0 mm.

Table 2 — Comparison of WZ and FZ Depths and Diameters for Both an Experimentally Measured Beam Profile and an Artificially Generated Top-Hat Profile

	Model Prediction		
	Measured Profile (mm)	Top-Hat Profile (mm)	Experiment (mm)
FZ depth	0.39	0.46	0.4
FZ diameter	0.85	0.68	0.89
WZ depth	0.43	0.5	0.43
WZ diameter	1.08	0.87	1.17

Table 3 — Focal Position vs. Absorptivity to Produce a Close Comparison between Theory and Experiment for the Conditions Shown in Fig. 5A and B

Focal Position (mm)	–5	–4	–3	–2	–1	0	1	2	3	4	5
Absorptivity (%)	35	33	33	33	37	30	28	28	30	25	25

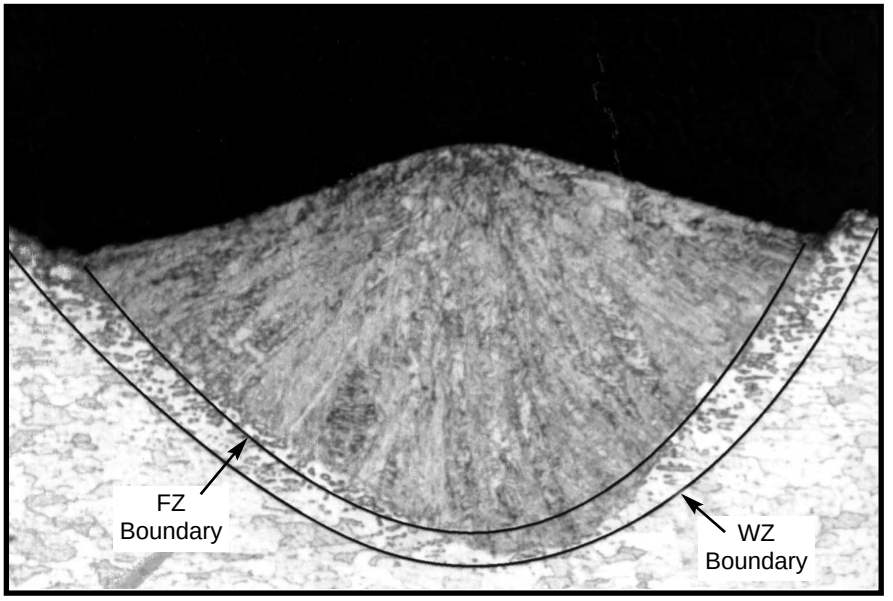

Fig. 4 — Micrograph of the cross section of a laser spot weld in 0.9-mm AISI 1006 steel showing ANSYS model predictions of the fusion and heat-affected zone boundaries. Laser conditions: 7 J, 3 ms, focus 0.

focal position, the maximum depth and diameter of the 1540 and 730°C temperature contours were measured. These measurements have been plotted in Fig. 5A and B, and may be compared directly with the experimental measurements of the FZ and WZ dimensions, respectively.

Previous work has shown that the deepest penetration associated with pulsed laser welding is achieved when the focal point is located 2–3 mm below the surface of the workpiece (Ref. 32). This value was based on the assumption that the minimum weld pool width corresponds to the focal point of the laser beam at the surface of the workpiece. This assumption was found to be misleading, particularly in the case of non-Gaussian beam profiles. In this study, an improved method of determining the focal point of the laser beam was employed. A Spiricon laser beam analyzer (LBA-100) was used to determine the optical focus of the laser beam. Using this analyzer, it was possible to measure the power distributed in the laser beam (beam profile) as a function of distance from the focusing lens. The position that gave the maximum power density was deemed the focal position. The laser beam profile on either side of this position was found to vary from a near-Gaussian profile (at positive focal positions) to donut-shaped profiles (at negative focal positions). The most accurate way of correlating spot welds with beam profiles was to compare these donut-shaped melt zones with the donut-shaped beam profiles. By performing the above focal scan on AISI 1006 steel to produce a series of individual spot welds, it was possible to match the diameter of the "annular" or donut-shaped beam profiles with the diameter of the annular spot welds. Therefore, from an optical point of view, it was found that under these laser conditions the point of maximum penetration actually occurred at 0 mm (Fig. 5A), *i.e.*, when the beam was focused at the surface of the workpiece. The finite element model corroborates this method of determining the focus. The predicted weld pool shapes are in excellent correlation with the experimental welds. These correlations are very poor if the previous method of determining the focal position is used.

The results in Fig. 5A and B verify this method of determining focus. It can be seen that the minimum melt diameter (FZ) is approximately 3 mm. The focal position at which the maximum power density is obtained does not yield the spot weld of smallest diameter due to the different intensity distributions at different focal positions.

Note that the estimation of thermophysical properties to be used as input to the model is a difficult task under these conditions, since a metal heated beyond its boiling point in less than 3 ms undergoes rapid changes and determining accurate material properties for such a wide range of temperatures is difficult. This task is more perilous when the temperature dependence of some important material properties is unknown. The absorptivity of the laser radiation is one such parameter.

The absorptivity of the 1.06-μm laser radiation by the workpiece is a complex function of a number of variables such as the nature of the surface, the level of oxidation, surface temperature, beam power density, beam angle of incidence, focal position of the laser beam relative to the workpiece surface, different amounts of absorption across the beam itself and the amount of plasma present. Since their precise roles have not been determined either experimentally or theoretically, an effective absorptivity for each focal position was incorporated into the analysis. This parameter includes, in an approximate way, all of these complex effects. The modification of energy input by convective movement is also included in this factor.

The variation of effective absorptivity with focal position is shown in Table 3. An effective absorptivity for each focal position was selected to achieve a close match between theory and experiment for just one set of results, in this case the

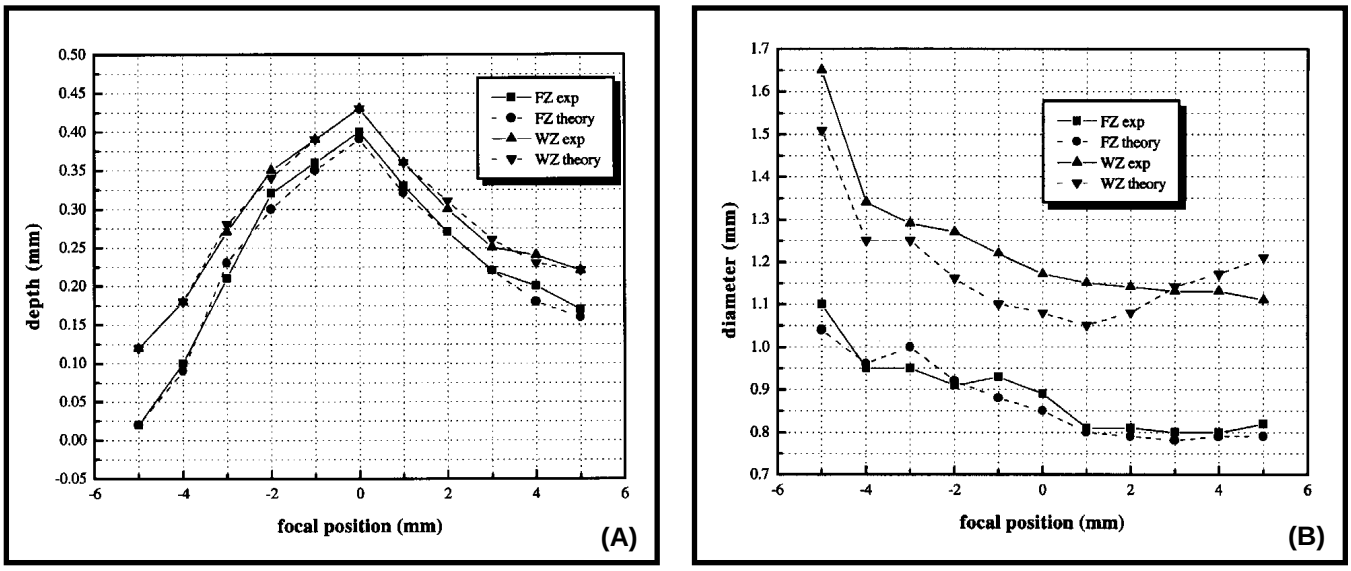

Fig. 5 — A — Measured FZ and WZ depths compared with model predictions based on changing absorptivities; B — measured FZ and WZ diameters compared with model predictions based on changing absorptivities.

maximum depth of the 730°C (1346°F) isotherm below the surface (WZ depth). The selected absorptivities compare well with previous estimations of the absorptivity of low-carbon steel to radiation of wavelength 1.06 μm (Ref. 33). When these values are used in the model, agreement within 10% between theory and experiment for FZ depth, FZ diameter and WZ diameter is achieved — Fig. 5.

It should be emphasized that the selection of an effective absorptivity for each focal position represents the only "calibration" factor in the model. Realistic temperature-dependent variables are used for all other thermophysical properties. The inclusion of experimentally determined beam profiles represents another important feature of the model. As the energy distribution at the surface of the workpiece is a strong function of both focal position and beam incidence angle, incorporation of these measured beam profiles is essential for accurate temperature calculations and weld pool shapes.

Conclusions

A three-dimensional finite element model of the heat flow during pulsed laser welding has been developed. This model is quite sensitive to the energy distribution and absorptivity of the laser beam. It has been applied successfully to spot welds on mild steel. Extension of this work is proceeding to fully understand the predictive ability and limitations of the model and its applicability to other materials and to a train of overlapping spot welds. Preliminary results have been reported elsewhere (Refs. 31, 34). A more direct check of the theoretical work, apart from the measurement of FZ and WZ dimensions and the consequent estimations of temperature contours, is the measurement of temperature as a function of time during laser welding. This may be achieved by measuring the temperature of the surfaces of sheet steel during welding. This temperature-time dependence may be directly compared with the appropriate output from the finite element model. The results of this work will be published at a later date.

Acknowledgments

The authors wish to acknowledge the financial support provided by the Cooperative Research Centre for Materials Welding and Joining, incorporating CSIRO Division of Manufacturing Technology, the University of Wollongong and BHP Research Port Kembla.

References

1. Rosenthal, D. 1946. The theory of moving sources of heat and its application to metal treatments. *Trans. ASME* 43 (11): 849–866.

2. Swift-Hook, D. T., and Gick, A. E. F. 1973. Penetration welding with lasers. *Welding Journal* 52(11): 492-s to 499-s.

3. Klemens, P. G. 1976. Heat balance and flow conditions for electron beam and laser welding. *J. Appl. Phys.* 47(5): 2165–2174.

4. Andrews, J. G., and Atthey, D. R. 1976. Hydrodynamic limit to penetration of a material by a high-power beam. *J. Phys. D: Appl. Phys.* 9(12): 2181–2194.

5. Cline, H. E., and Anthony, T. R. 1977. Heat treating and melting material with a scanning laser or electron beam. *J. Appl. Phys.* 48(9): 3895–3900.

6. Davis, M., Kapadia, P., and Dowden, J. 1986. Modelling the fluid flow in laser beam welding. *Welding Journal* 65(7): 167-s to 174-s.

7. Weckman, D. C., Mallory, L. C., and Kerr, H. W. 1989. A technique for the prediction of average weld pool width and depth for GTA welds on stainless steels. *Zeitschrift für Metallkunde* 80(7): 459–468.

8. Steen, W. M., Dowden, J., Davis, M., and Kapadia, P. 1988. A point and line source model of laser keyhole welding. *J. Phys. D: Appl. Phys.* 21(8): 1255–1260.

9. Akhter, R., Davis, M., Dowden, J., Kapadia, P., Ley, M., and Steen, W. M. 1989. A method for calculating the fused zone profile of laser keyhole welds. *J. Phys. D: Appl. Phys.* 22(1): 23–28.

10. Dowden, J., Kapadia, P., and Postacioglu, N. 1989. An analysis of the laser-plasma interaction in laser keyhole welding. *J. Phys. D: Appl. Phys.* 22(6): 741–749.

11. Finke, B. R., Kapadia, P. D., and Dowden, J. M. 1990. A fundamental plasma based model for energy transfer in laser material processing. *J. Phys. D: Appl. Phys.* 23(6): 643–654.

12. Tosto, S. 1993. Modelling of the thermal field induced by laser irradiation in the presence of heat sinks or sources. *Lasers in Engineering* 2(1): 61–74.

13. Kaplan, A. 1994. A model of deep penetration laser welding based on calculation of the keyhole profile. *J. Phys. D: Appl. Phys.* 27(9): 1805–1814.

14. Mazumder, J., and Steen, W. M. 1980. Heat transfer model for CW laser material processing. *J. Appl. Phys.* 51(2): 941–947.

15. Paul, A., and DebRoy, T. 1988. Free surface flow and heat transfer in conduction mode laser welding. *Metall. Trans.* 19B: 851–858.

16. Molino, G., Penasa, M., Perlini, G., Tiziani, A., and Zambon, A. 1990. Thermal modelling of the laser welding process using

a realistic power distribution of the beam. *Proc. 3rd European Conf. on Laser Treatment of Materials*. Eds. H. Bergmann and R. Kupfer, Sprechsaal Publishing Group, pp. 195–205.

17. Gratzke, U., Kapadia, P. D., and Dowden, J. 1991. Heat conduction in high-speed laser welding. *J. Appl. Phys. D: Appl. Phys.* 24(12): 2125–2134.

18. Aden, M., Beyer, E., Herziger, G., and Kunze, H. 1992. Laser-induced vaporization of a metal surface. *J. Appl. Phys. D: Appl. Phys.* 25(1): 57–65.

19. Dowden, J., Chang, W. S., Kapadia, P., and Strange, C. 1991. Dynamics of the vapour flow in the keyhole in penetration welding with a laser at medium welding speeds. *J. Appl. Phys. D: Appl. Phys.* 24(4): 519–532.

20. Zacharia, T., David, S. A., Vitek, J. M., and DebRoy, T. 1989. Heat transfer during Nd:YAG pulsed laser welding and its effect on solidification structure of austenitic stainless steels. *MetalI. Trans.* 20A: 957–967.

21. Russo, A. J., Akau, R. L., and Jellison, J. L. 1990. Thermocapillary flow in pulsed laser beam weld pools. *Welding Journal* 69(1): 23-s to 29-s.

22. Vishnu, P. R., Li, W. B., and Easterling, K. E. 1991. Heat flow model for pulsed welding. *J. Mat. Science and Tech.* 7(7): 649–659.

23. Gellert, B., and Egli, W. 1988. Melting of copper by an intense and pulsed heat source. *J. Appl. Phys. D: Appl. Phys.* 21(12): 1721–1726.

24. Jette, A. N., and Benson, R. C. 1994. Modeling of pulsed-laser cleaning of metal optical surfaces at cryogenic temperatures. *J. Appl. Phys.* 75(6): 3130–3141.

25. Arutyunyan, R. V., Baranov, V. Y., Bol'shov, L. A., Malyuta, D. D., Mezhevov, V. S., and Pis'mennyi, V. D. 1987. Thermo-hydrodynamic models of the interaction of pulsed-periodic radiation with matter. *Sov. J. Quant. Elect.* 17(2): 163–168.

26. Brown, S., and Song, H. 1992. Finite element simulation of welding of large structures. *J. Eng. Ind.* 114(11): 441–451.

27. Kim, C. S. 1975. Thermophysical properties of stainless steels. Technical Report ANL-75-55. Argonne National Laboratory, Argonne, Ill., pp. 1–24.

28. Vinokurov, V. A. 1977. *Welding Stresses and Distortion*. The British Library, Boston Spa, England, pp. 118–119.

29. ANSYS Revision 5.0 User Manual. 1992. pp. 31–34.

30. Frewin, M. 1997. Experimental and theoretical investigation of tandem laser welding. Ph.D. thesis, University of Wollongong, NSW, Australia.

31. Scott, D. A. 1997. Tandem fibre-optic laser welding head. *CRC Project 93-16 Final Report*. Co-operative Research Centre for Materials Welding and Joining, Wollongong, NSW, Australia.

32. Frewin, M., and Scott, D. A. 1995. Numerical and experimental investigation of pulsed Nd:YAG laser welding. *Proc. ICALEO '95*. Eds. J. Mazumder, A. Matsunawa, and C. Magnusson, Laser Institute of America, pp. 904–913.

33. Zacharia, T., David, S. A., Vitek, J. M., and DebRoy, T. 1989. Heat transfer during pulsed laser welding and its effect on solidification structure of austenitic stainless steels. *MetalI. Trans.* 20A: 957–967.

34. Frewin, M., Dunne, D., and Scott, D. A. 1998. Structural evolution of pulsed Nd-YAG laser welds of AISI 1006 steel. *Science and Technology of Welding and Joining* 3(3).